STUDY OF STORM TIDE MODELING IN THE PEARL RIVER ESTUARY

Edward Qiang Shen[1]

By reproducing storm tides during nine historical typhoons in the Pearl River Estuary against observations, this paper presents a data-model comparison approach to quantify the uncertainties of three parameters of Holland (1980) parametric wind model. The wind reduction factor that represents effects of mountains and skyscrapers surrounding the estuary may be estimated by finding the minimum RMSE in simulated storm tide peak elevation. The radius to maximum winds can be efficiently adjusted according to observed pressures through the exponential distribution of atmospheric pressure field; and the peakedness is verified on the basis of maximum wind speed versus pressure drop relations. By applying these parameters with the wind model, storm tides in the estuary can be effectively simulated, except for wind conditions where most of the estuary is within the maximum wind radius and winds there are significantly affected by the mountainous lands. Wave setups are noticeable when typhoons made landfall on the right bank of the estuary. As a prerequisite for good model performance, the grid size somewhere in a storm tide model should be smaller than the minimum spacing among soundings points at that location in order to effectively produce the model bathymetry described by the soundings data.

Keywords: parametric wind model; storm tide simulation; estuary; wave setup; model grid size.

INTRODUCTION

The Pearl River Estuary (PRE) is the estuary of China's second largest river. It is hit by 5~6 tropical cyclones every year on average. Among them at least two are typhoons; they are the tropical cyclones with maximum sustained surface winds exceeding 117 km/h near their centers. Storm tide modeling is the simulation of astronomical high tides encountering storm surges and waves generated by typhoons. It has become an increasingly important tool in the prediction, prevention, and mitigation of coastal flood disasters. Some of researches in this area came into view after the PRE was heavily hit by super Typhoon Hato in 2017. A key feature of these studies is the application of numerical weather prediction models to provide typhoon wind and pressure fields as inputs to storm tide models. Hydrodynamic models of storm tides have been developed to be very reliable over recent decades. The accuracy of storm tide simulation is determined mainly by surface wind and pressure fields in addition to bathymetry; and the recent trend is to develop a tide-surge-wave coupled system (Kohno et al. 2018).

In a comparative study of flooding field survey and storm tide modeling, for the period when Typhon Hato struck Macao, pressure and wind fields from results of a numerical weather model (WRF) were used as the input to drive a tide–surge–wave coupled hydrodynamic model (Li et al. 2018). The data–model comparisons showed that the numerical model package may capture all key features of the event, such as wind fields, storm tide levels, and inundation depths. But the discussion about underestimated inundation depths is limited only to draw an inference from topographic modeling errors, without a quantitative evaluation of model performance and wave effects on storm tide levels.

In a recent study of tide-surge interaction in the PRE during Typhoon Hato (Zheng et al. 2020), a wind field and pressure dataset obtained from a similar numerical weather model was also used. These data were found to be difficult to describe the vortex structure at the center of the typhoon, seriously underestimating the wind speed near the center. Blended atmospheric forcings by inserting winds and pressures, which was calculated by the Holland (1980) parametric wind model, into the original model data, were therefore used instead. The air pressure and wind fields near the typhoon eye were calculated by the Holland (1980) model, and far from the center it was formulated by the dataset. Although significant improvements in predicted water levels are obtained by using the blended data, some noticeable discrepancies are still observed in modeled winds and water levels. This is likely due to missing wave-induced setup in the model simulation, and that the parametric wind model does not account for the structural changes and wind reduction caused by local land topography.

Further, the grid sizes of above two hydrodynamic models, that were used for the storm tide simulation in the same waters during the same typhoon, are also very different. The former has an unstructured grid with horizontal resolution about 1 km over the shelf to 20 m inside the PRE, while the latter's is about 300 ~ 500 m inside the PRE. This raises a new question about how to determine an appropriate grid size for the storm tide model in a specific water area.

Parametric wind and pressure models, such as the Holland (1980) model, remain useful and will continue to be utilized in storm surge simulation (Kohno et al. 2018), as they may provide appropriate tropical cyclone intensities, give better wind and pressures inputs, and facilitate track adjustment. The three parameters of the model, namely radius to maximum winds (R_{mw}), peakedness (B), and surface

[1] Guangzhou Maritime University, No. 101, Hongshan 3rd Road, Huangpu District, Guangzhou, 510725, China. Arup (HK) Ltd. Email: edward.qiang.shen@gmail.com

wind reduction factor (K_m), which are subject to site-specific terrain or latitude, however, are determined empirically and contain large uncertainty. For instance, K_m must be used to transfer gradient level winds to the standard 10-m elevation above the sea. The combination of the empirical boundary layer model and the variable cap on the sea surface drag coefficient yields K_m over the ocean is about 0.67 to 0.74, varying with both storm size and intensity. Over the land, there is more reliance on models to estimate the characteristics of tropical cyclone boundary layer. This suggests that K_m shall be further adjusted by about 15 ~ 20% over the sea-land transition area (Vickery et al. 2009).

It is generally accepted that the magnitude of R_{mw} is negatively correlated with the central pressure difference (Δp), so that more intense storms (larger Δp) have smaller R_{mw} than the weaker storms. The R_{mw} also increases with increasing latitude. There is significant scatter of the data about the modeled R_{mw} - Δp relationships (Vickery et al. 2009). Although R_{mw} is now typically being recorded in best track datasets, it remains difficult to estimate for all cases. In practice, R_{mw} is relatively easily estimated by satellite-based techniques only when eye features exist. Therefore, it is recommended to develop historical datasets, technologies and methods to improve the estimates of R_{mw}, and the quantification of the relationship between the variations of R_{mw} and minimum sea level pressure (Knaff and Harper 2012).

Harper and Holland (1999) suggested an empirical relation for B, making B a direct function of storm central pressure. Both Powell et al. (2005) and Vickery and Wadhera (2008) found that B decreases with increasing R_{mw} and latitude, and is weakly dependent on the central pressure, in contrast to the suggested relationship. Holland (2008) devised a new empirical relation for relating maximum winds to central pressure in tropical cyclones. He determined a derivative of the Holland B parameter, B_s, which relates the pressure drop directly to surface winds. This parameter B_s is a function of pressure drop at the center of the tropical cyclone, intensification rate, latitude, and translation speed.

Figure 1. Major topographic features surrounding the PRE and main observation stations in the estuary

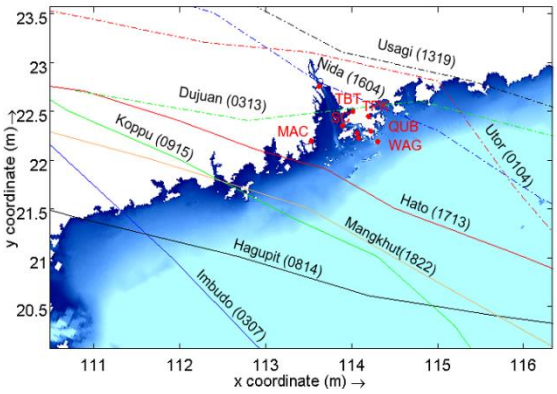

Figure 2 - Tracks of nine representative typhoons

The PRE is surrounded by alluvial plains, mountains, and skyscrapers (Fig. 1). On the left bank of the estuary, there are Tai Mo Shan, Hong Kong's highest peak at an altitude of 957 m, Lantau Island (peak 934 m), and Wutong Mountain in Shenzhen (peak 944 m). On the right bank, there are Naobei Mountain (peak 457 m), Huangyang Mountain (peak 500 m) in Zhuhai, and Wugui Xiongfeng in Zhongshan. There are also several large and small islands scattered near and inside the estuary, such as Dangan Island (peak 400 m), that crosses the offshore waters southeast of the estuary. When a typhoon moves from the sea to the land, especially when it makes landfall, wind fields are modulated by orographic effects, thereby influencing the generation and distribution of storm surges in the estuary, and the value of surface wind reduction factor.

The estuary is subject to the combined action of tide, wave, and river runoff. According to the extent of their respective influences on estuarine hydrodynamics, the estuary can be divided into three sections, namely upper, middle, and lower, along its longitudinal direction from north to south (Fig. 1). The upper section comprising waters above NS (Nansha) is mainly subject to the action of tide and river runoff. The water area below NS to CW (Chiwan) and DWW (Dawuwan) is the middle section, where tides, runoffs, and waves have varying extents of influence. From there, further south to Hong Kong and Macau, the waters in between is the downstream section, about 40 km long and 30 km wide. In this water area, tide and wave forcings are strong but the influence of river runoff is relatively weak. This is the key waters the study focuses on.

Against this background, the objective of this study is to investigate the applicability of parametric wind model for storm tide simulation in the PRE, including the following tasks: (1) by modeling storm tides during the passage of selected nine historical typhoons and quantitively evaluating the model performance, to explore how the three parameters can be determined using observed wind, pressure, and seal level data; (2) to examine effects of grid size of a hydrodynamic model on the model performance; and (3) to test effects of waves on storm tide levels in the lower section of the PRE.

Of the nine representative typhoons, five made landfall on the right bank of the PRE, and four on the left bank (Fig. 2). Storm tides produced during these typhoons used to cause serious floodings in cities along and upstream of the PRE; at the same time, there exist relatively complete and reliable pressure, wind, and water level data recorded during the typhoons so that the data can be used to verify the modeling results.

The track and intensity datasets of the selected nine typhoons are quoted from Tropical Cyclone Annual Report published by the Hong Kong Observatory (HKO); it includes the position of the typhoon center, the estimated minimum central pressure, and the maximum sustained surface winds every six hours. Hourly water level, wind speed, air pressure and wave data recorded at main observation stations in the PRE (Fig. 1), that are cited in this study, were mainly acquired from the HKO. Seabed bathymetry of the PRE and adjacent waters was obtained from digital nautical charts with a scale ranging from 1:15,000 to 1:250,000.

Throughout this paper, water levels refer to the Hong Kong chart datum. Maximum sustained surface winds refer to wind speeds averaged over a period of 10 minutes. Hourly mean winds are winds averaged over a 60-minute interval ending on the hour and pressures refer to the mean sea level. The 10-minute average wind speed at 10 m elevation above the sea is uniformly adopted in the study, thus winds other than this were converted to this wind format.

WIND SIMULATION

Maximum Wind Radius and Peakedness

The parametric pressure and wind fields are generated on a spiderweb type grid with a radius of 600 km and the grid spacing of 10 km both in the radial and the circumferential directions. The surface peakedness B_s is evaluated by using Eq. (A5) in the Appendix, where the maximum sustained surface winds and the minimum central pressure are taken from the typhoon track and intensity datasets. It is clear that B_s varies with the typhoon intensity, and that with the known B_s, the pressure calculated at a given distance from the center of tropical cyclone decreases with increasing R_{mw}.

The rationality of R_{mw} for the selected nine typhoons (Table 1) can be justified by comparing the difference between modeled and observed pressures, especially between the minimum pressures, at station WAG (Fig. 1). This station is about 5 km from Hong Kong Island, and is the closest to the open sea among existing stations in the PRE. Recorded winds and pressures at the station are generally considered to be relatively less affected by the land. In justification, the default R_{mw} equal to 56 km (Lau and Chan 2017) is tested first, then it is adjusted and finalized according to the discrepancy found and by reference to HKO's weather information reported during the passage of typhoons.

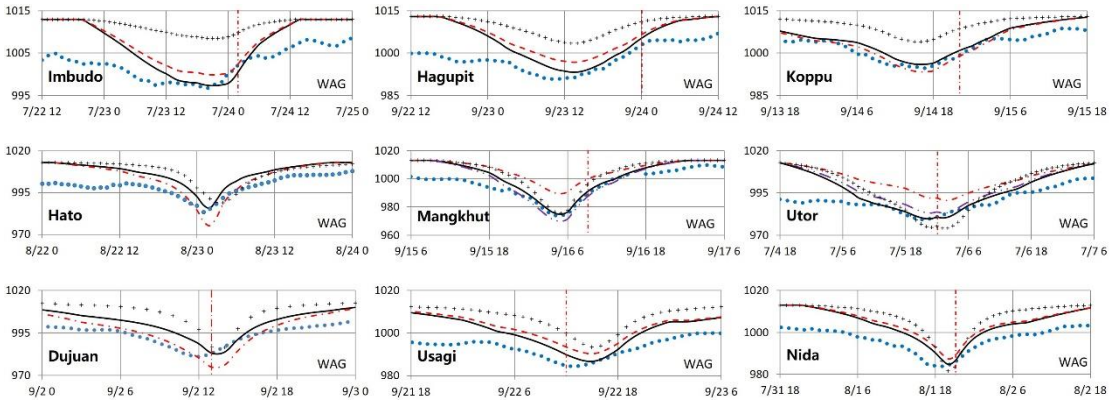

Legend: ..... observed —— modeled (R_{mw} see Table 1) - - - - - modeled (R_{mw}=45 km) _ . _ . _ modeled (R_{mw}=56Km) _ . . _ modeled (R_{mw}=120Km) + + + + + modeled (B calculated by Eq. [A4], R_{mw} see Table 1)
dashed vertical line – landfall time

Figure 3 - Comparison of parametric pressures with observed pressures at station WAG

Table 1. Minimum relative distances (r_{min}/R_{mw}) from the center of typhoon to main monitoring stations in the PRE

Typhoon	R_{mw} (km)	K_L	Observation Station				
			MAC	TBT	QUB	WAG	SC
Landfall on the right bank							
Imbudo	56	0.70	3.8	4.9	4.8	4.8	4.5
Hagupit	56	0.65	2.7	3.5	3.2	3.1	3.2
Koppu	45	0.65	2.0	3.1	2.8	2.7	2.7
Hato	38	0.75	0.7	1.9	1.7	1.5	1.4
Mangkhut	100	0.75	0.7	1.2	1.1	1.1	1.0
Landfall in the left bank							
Utor	160	0.55	0.6	0.3	0.5	0.5	0.5
Dujuan	35	0.55	0.9	0.1	0.8	1.2	0.5
Usagi	56	0.50	1.9	1.1	1.4	1.6	1.5
Nida	56	0.50	1.2	0.3	0.5	0.7	0.7

(r_{min} is the minimum distance from observation station to the typhoon center)

We can see that, by examining the difference between modeled and observed pressures at station WAG during Typhoons Imbudo, Hagupit, Usagi, and Nida (Fig. 3), pressures modeled by using the default R_{mw} is closer to the observations than using other radii, especially the minimum pressure. But during Typhoon Koppu, R_{mw} equal to 45 km gives better results. Similarly, the discrepancy found during Typhoons Hato and Dujuan is reduced by adjusting the default R_{mw} to 38 km and 35 km respectively.

According to information provided by HKO (2001, 2018), Typhoon Utor's circulation was extensive, its radius reached some 1000 km and a large and irregular eye was discernible on satellite imagery; Typhoon Mangkhut was characterized by its extensive circulation as well. This means that these two typhoons have a larger radius to maximum winds. By testing for different values, R_{mw} for Typhoons Utor and Mangkhut is likely about 160 km and 100 km respectively as it works best in reducing the difference found between modeled and observed minimum pressures.

We can also see that the agreement between modeled and observed pressures is much better when the peakedness B_s is calculated by using Eq. (A5) instead of Eq. (A4), as shown in Fig. 3; apparently, the latter is not applicable to the atmospheric environment in the PRE.

Wind Reduction Factor

The wind field of typhoon will be modulated mainly by mountains and skyscrapers around the PRE when the storm moves from the sea to the land, causing winds over the sea to decrease. To apply Holland (1980) parametric wind model (see details in the Appendix) for storm tide simulation in the PRE, a new coefficient K_L is introduced to take account of these effects, then from Eq. (A2), the affected surface winds due to orographic effects can be expressed as

$$V_s = K_L \sqrt{\frac{B_s(p_{ns} - p_{cs})}{\rho_s}\left(\frac{R_{mw}}{r}\right)^{B_s} exp\left[-\left(\frac{R_{mw}}{r}\right)^{B_s}\right] + \frac{r^2 f^2}{4}} - \frac{rf}{2} \quad (1)$$

The storm surge is more sensitive than the wind to the change of wind reduction factor as the surge height is proportional to the square of the wind speed, the factor may be derived from the calibration of storm tide peak. This means that we can find K_L by calculating the minimum value of root mean square error (RMSE) of highest storm tide levels at monitoring stations in the PRE, that is,

$$min\ RMSE = \left[\frac{1}{N}\sum_{i=1}^{N}(\eta(K_L)_{max\ model} - \eta_{max\ obs})^2\right]^{\frac{1}{2}} \quad (2)$$

where $\eta(K_L)_{\max model}$ and $\eta_{max\ obs}$ are the simulated and observed highest storm tide levels, the former varies with different K_L; and N is the number of observation station. In the PRE, these stations are some 80 km apart from west to east, and 30 km from north to south, the derivation of K_L, as shown in Eq. (2), is based on the average performance of modeled storm tide peak elevations in the PRE, so the derived K_L shall represent the overall average effect of mountains and skyscrapers around the estuary, especially the effect on maximum winds in the PRE.

As a result, the wind modeled by applying K_L is generally stronger than the observation in places where the wind field is greatly affected; conversely where the wind field is less affected, the modeled wind is likely weaker than the observation. Not only that, but the wind conditions at each observation

station in the PRE are also affected by the local topography, and the wind field changes in different ways. These characteristics of the difference between modeled and observed winds make it difficult to evaluate the performance of parametric wind model by comparing how well the simulated winds fit the observation. Whereas, the rationality of K_L may be verified indirectly by the characteristics of difference in winds observed at different locations.

For example, station SC is located inside the PRE, 46 km away from station WAG, but separated by islands (Fig. 1). These two stations are approximately in the same distance to the center of selected nine typhoons, so the predicted winds are similar. As winds near station SC are affected greatly by the surrounding islands, the recorded winds there during typhoons shall weaken and be weaker than the modeled winds. This inference is consistent with what found in observed winds when Typhoons Mangkhut and Usagi approached the two stations. Comparing to the modeled winds, the winds observed at station SC weakened significantly near the peak, while the observed winds at station WAG were close to the modeled winds (Fig. 4).

The rationality of K_L can also be verified by examining the patterns of errors in modeled winds at an observation station for different times when a storm approaches and leaves the station. According to the study of Willoughby and Rahn (2004), if the storm is far away from an observation station, that is, relative distance $r/R_{mw} > 3$, where r is the distance between storm center and observation station, the wind predicted by Holland (1980) model at the station is underestimated; and the difference between the predicted and observed winds increases rapidly with increasing the distance. The model is also often impossible to accurately reproduce the core wind structure in hurricanes; the areas of strong winds in the eyewall and of nearly calm winds at the vortex center are too wide.

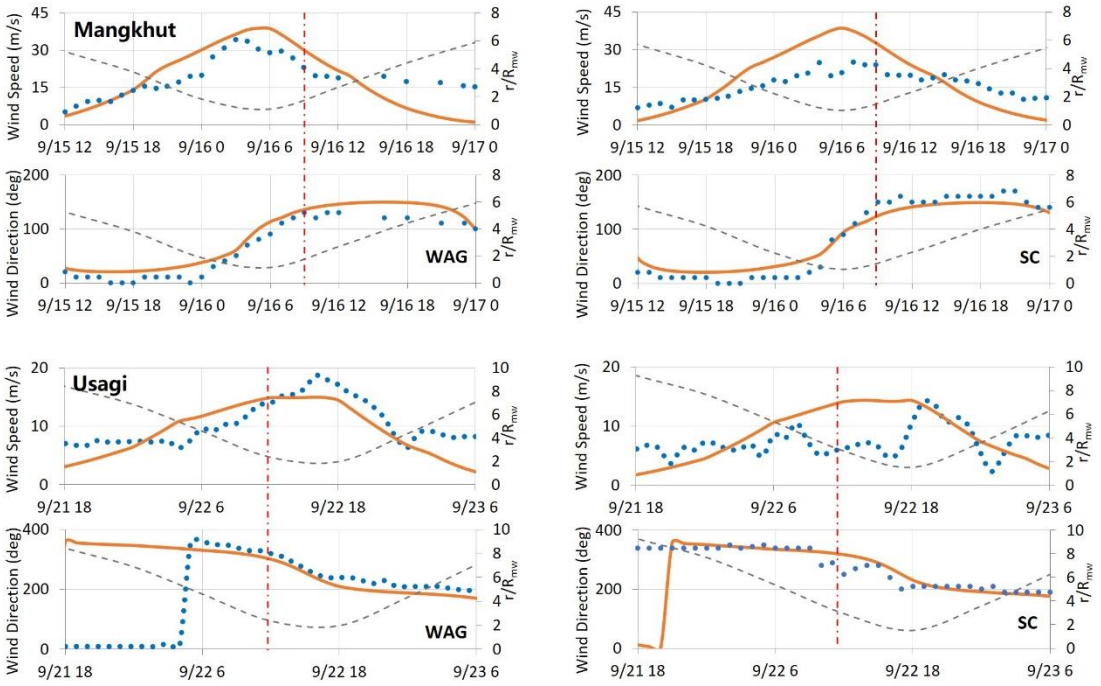

Legend: ..... observed —— modeled - - - - - r/R_{mw} dashed vertical line – landfall time

Figure 4 - Comparison of parametric winds with observed winds at stations WAG and SC (UTC Time, 10-minute average wind at 10 m elevation above the sea)

By comparing the difference between the predicted and observed winds at station WAG during Typhoon Mangkhut (Fig. 4), we note that the pattern of this difference is not consistent before and after the wind peak although the storm is far away from the station and r/R_{mw} from the station is the same. For instance, the difference pattern found at 18:00 on September 15 before the wind peak is not as significant as that at 16:00 on September 16 after the wind peak. But further check of winds recorded at the two positions reveals that, the wind direction changed by more than 90 degrees before and after the wind peak, this explains why the difference pattern before and after the wind peak is not consistent.

Before the peak, far away from the station northeast winds came from the land to the sea (or sea-land-sea, Fig. 5a), and were greatly modulated by mountains and skyscrapers. The recorded winds weakened, so the difference between modeled and observed winds decreases. After the peak, the storm left the station and winds, that blew to the PRE in the southeast direction from the sea to the land (Fig.

5b), were less affected by the topography. This wind condition is similar to that of Holland model, i.e. the wind over the sea; therefore, the deficiency of the model is obvious. The above discussions show that K_L derived from Eq. (2) is reasonable and effective in estimating the influence of natural and built environment surrounding the PRE on wind fields of typhoons.

The patterns of errors in modeled winds far from the storm center during Typhoon Usagi and other selected typhoons, are similar, too. Being different from the wind condition during typhoons that made landfall on the right bank, the wind direction in the PRE during typhoons that made landfall on the left bank, such as Typhoon Usagi, changed gradually from northwest to southwest when the typhoons approached and left the PRE.

In calculating K_L from Eq. (2), we note that highest storm tide levels during typhoons that made landfall on the right bank of the PRE, are more sensitive to the change of K_L. For every 0.05 increment of K_L, the highest storm tide level increases about 0.06 m to 0.24 m at different stations. For instance, during Typhoon Mangkhut, the peak water level at station MAC may increase by 0.23 m, while the corresponding wind speed increases only by about 2 m/s. During typhoons that made landfall on the left bank, the increase in peak water level by an increment of 0.05 is about 0.01 m to 0.09 m at different stations.

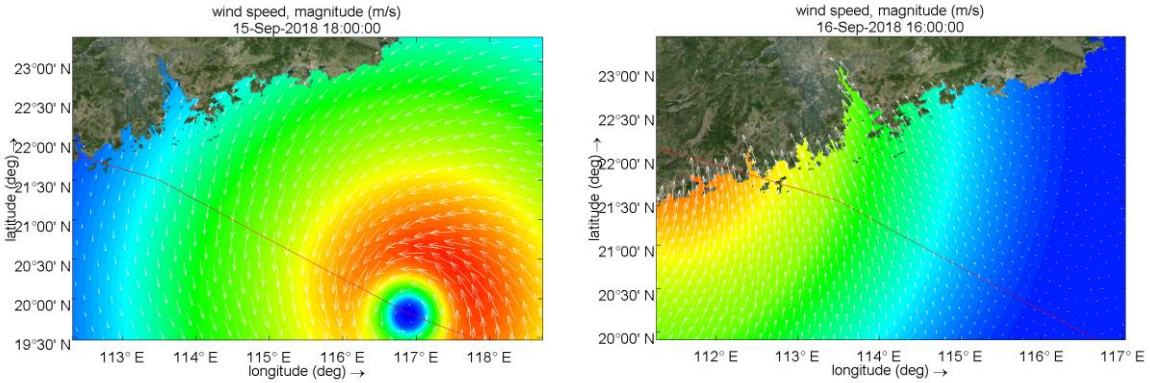

(a) approached the PRE:
Pc=945 hPa, Vs max=52 m/s, r/R_{mw}=3.78

(b) left the PRE:
Pc=972 hPa, Vs max = 34 m/s, r/R_{mw}=3.85.

Figure 5 - Modeled wind fields of Typhoon Mangkhut when it approached and left the PRE

When typhoons made landfall on the left bank, the peak winds recorded in the PRE occurred after the landfall; while during typhoons which made landfall on the right bank it took place before the landfall (see Fig. 4). This means that the peak winds, which likely produced highest storm tides in the PRE during typhoons that made landfall on the left bank, had experienced bottom resistance changed from the sea to the land, and then from the land to the sea. Winds were affected more by the topography. As a result, K_L is smaller than that found for typhoons making landfall on the right bank (right bank: 0.65 ~ 0.7, left bank: 0.5 ~ 0.55). This is comparable to those derived from hurricane boundary layer models with a capped representation of marine drag coefficient (Vickery et al. 2009).

SET-UP OF STORM TIDE MODEL

Model Domains and Grids

Two regular grid layouts are used to establish regional and local models in order to examine the influence of model grid size on the performance of storm tide simulation. The domain of the regional model approximately covers waters with a radius of about 800 km from the PRE (Fig. 6). This is also the zone that a warning signal will be issued by HKO when the center of a tropical cyclone moves across the zone border. The open boundary of regional model should be far enough away from the PRE to ensure that effects of changes in boundary conditions, which are likely caused by typhoons inside or outside the model, on waters of the PRE can be ignored. The regional model has the grid size of 600 ~ 1000 m in the lower reach of the PRE.

The local model covers the entire PRE. The position of its open boundary is determined according to the requirement that the ratio of the length of open boundary in waters of 50 m deep or more to the total length of the open boundary should not be less than 50% (Shen 2022), in order to minimize the effect of deficiency in open boundary conditions.

To find a proper grid size for the local model, we first examine an example of a navigational channel with a side slope of 1:10 and soundings data that represent the channel (Fig. 7a). The minimum spacing among these soundings points is 50 m. For a set of regular grids with varying grid sizes of 5, 40, 50 and 100 m, different depth files are produced by applying Quickin interpolation module of Delft3D and then are used to plot channel cross sections (Fig. 7b). If the grid size is larger than 50 m, i.e. the minimum spacing among the soundings points, the simulated water depths no longer properly shape the channel cross section. Only when the grid size is smaller than the minimum spacing can the cross section be properly delineated by the modeled water depth. If the grid size is 5 m, the resulting water depths map the cross section almost perfectly, but the difference is not significant compared to that with a grid size of 40 m, which consumes much less digital resources.

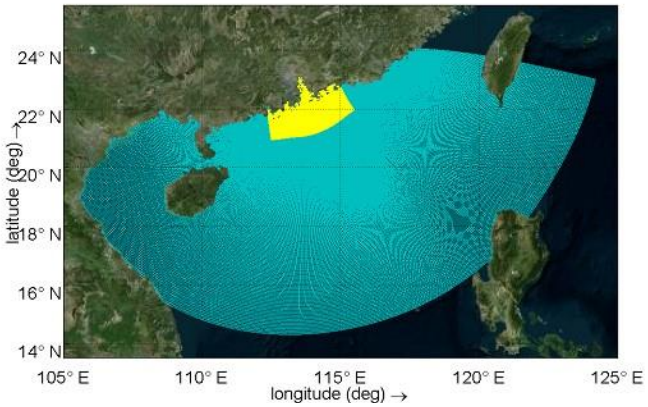

Figure 6 - Regional and local model domains

From this example, we may conclude that for a set of soundings data only when the grid size somewhere in a model is smaller than the minimum spacing among the sounding points at that location, the model grid can effectively produce the bathymetry described by the soundings data. An optimal grid shall be the one that not only well produces the bathymetry from given soundings data, but also has a lower computational expense. As a result, the grid size of the local model in the lower reach of the PRE shall be 150 ~ 400 m.

Model Boundary Conditions

Along the open boundary of the regional model, tide forcings is specified by astronomical tide constituents, which consist of 13 major tide components (M2, S2, N2, K2, K1, O1, P1, Q1, MF, MM, M4, MS4 and MN4) obtained from a global tide model (Egbert and Erofeeva 2002). On the boundary, a mean tide level is determined by calibration of tidal levels over the month during which the selected typhoons occurred; it varies depending on the appearance time of each selected typhoon. Due to the large domain of the regional model, tide-generating forces inside the model are considered. The local model has its open boundary nested in the regional model, then water level and flow velocity boundary conditions are extracted from regional model runs.

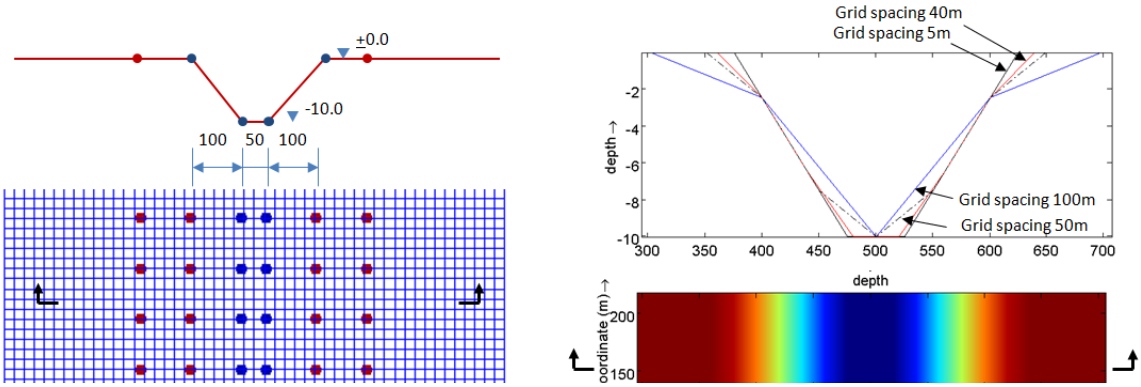

(a) Channel cross-section and soundings (b) Cross-sections mapped by different grid sizes

Figure 7 - Illustration of underwater terrain produced by model grids with different grid sizes

The flow-wave interaction and wave effects on storm tide levels are simulated by the Delft3D flow-wave coupling system. The regional wave model has similar domain and grid size as that of the regional flow model. A local fine grid same as that for the local flow model is nested in the regional wave model. As the study focuses on storm time simulation in the lower reach of the PRE, no river runoffs are incorporated into the flow model.

Important Model Input Parameters

Winds blowing over a sea create tangential stress on the sea surface, generating drift current and wave. The tangential stress is normally expressed as a quadratic drag law: $\tau = C_D \rho_a w^2$, where C_D is the wind drag coefficient, ρ_a is the air density, and w is the wind speed. Recent studies have shown that the drag coefficient does not increases monotonically with increasing surface wind speed. Observations and laboratory experiments (Powell et al. 2003; Jarosz et al. 2007) have indicated that the magnitude of the drag coefficient levels off at a wind speed of about 30 m/s, and then decreases with further increase of the wind speed. Above a wind speed of approximately 30 m/s, the stress above the air-sea interface starts to saturate. As recommended in the Delft3D modeling system, in this study when the wind speed (10 m above sea level) increases from 0 to 28 m/s, C_D linearly increases from 0.00115 to the peak value 0.0031; when the wind speed is greater than 28 m/s and less than 60 m/s, C_D linearly decreases from 0.0031 to 0.0015; and C_D remains constant when the wind speed is greater than 60 m/s.

The seabed roughness coefficient is optimized by calibration of tidal levels for the regional and local mode. The Chezy coefficient of 55 is applied for the regional model. The local model uses the Manning roughness coefficient of 0.02, this is similar to that used in the Pearl River Delta water quality model (Delft Hydraulics 2008).

STORM TIDE SIMULATION

Tide Simulation

The performance of a storm tide model depends not only on the simulation of wind field, but also on the tidal simulation. The error of mean water level (MWL) alone in the tide simulation can add error considerably to the highest storm tide level. The MWL at different monitoring stations in the PRE varies spatially, thus it is difficult to effectively simulate the MWL at different stations by specifying a single MWL on the open boundary of a tidal model. For this reason, in the calibration of tide model, three monitoring stations, namely MAC, TBT and QUB (Fig. 1), are selected as control stations. Station MAC is located in the western part of the PRE, stations QUB and TBT are positioned in the eastern and northeastern parts of the PRE; these stations are some 80 km apart from west to east, and 30 km from north to south. The MWL on the open boundary is determined by finding the one that has the minimum value of RMS errors in predicted mean water levels at the control stations.

The regional and local tidal models were calibrated against hindcast water levels for time periods during which the nine typhoons occurred. Calibration results of both models show that RMS errors of simulated tidal levels at control stations are less than 0.2 m, except that it is slightly larger (0.23m) only at TBT station for lack of measured data. The averaged errors of MWL at control stations are all within 0 ~ 0.03 m.

Storm Tide Simulation

Apart from the wind parameters B_s and R_{mw} of a typhoon, a set of K_L is generated with an increment of 0.05 to produce different wind fields as inputs to a set of storm tide simulations; the K_L that satisfies Eq. (2) can be ascertained by finding the minimum RMSE in storm tide peak levels over the control stations. By this way the wind reduction factors of nine typhoons are found for the regional and local model respectively (Table 2). When changes in storm tide peak elevations caused by K_L are too small, or the calculated highest storm tide levels deviate significantly from the observation, the minimum value of Eq. (2) may not exist.

Comparing wind reduction factors of the regional and local models (Table 2), one sees that for the regional model, values of K_L are relatively large, and so are the minimum RMS errors in Eq. (2). The difference between the two models can be further identified by comparing the modeled peak water levels with the observations at control stations during nine representative typhoons; as illustrated in Fig. 8, we see that the peak levels modeled by the regional model are mostly lower than the observed with considerable deviation. In addition, no minimum value was found from Eq. (2) in the storm tide simulation for Typhoon Dujuan; the values of K_L derived from the regional model runs diverge apparently for the selected nine typhoons. Thus, the reliability of the K_L is low.

The difference found in storm tide peak simulation shows that the local model surpasses the regional model, and the derived K_L is representative. Because the finer grid of the local model is able to capture

soundings data effectively, the bathymetry is well produced; and it is also able to adapt to space and time varying winds of a storm. Studies have shown that the grid properties influence the simulated water levels by way of bathymetry accuracy, numerical friction, and numerical viscosity (Bomers, Schielen, and Hulscher 2019).

Table 2. K_L and corresponding minimum RMSE for regional and local model

Typhoon	R_{mw}	Local model		Regional model	
		K_L	min RMSE	K_L	min RMSE
Imbudo	56	0.70	0.10	0.75	0.16
Hagupit	56	0.65	0.15	0.70	0.18
Koppu	45	0.65	0.09	0.70	0.09
Hato	38	0.75	0.12	0.80	0.30
Mangkhut	100	0.75	0.03	0.95	0.02
Utor	160	0.55	0.04	0.55	0.40
Dujuan	35	0.55	0.32	n/a	n/a
Usagi	56	0.50	0.09	0.50	0.38
Nida	56	0.50	0.18	0.75	0.18

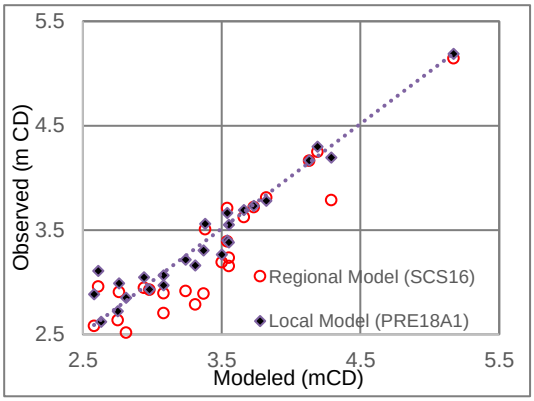

Figure 8 - Comparison between modeled and observed storm tide peak elevations

The performance of storm tide simulation is evaluated for a three-day period surrounding the peak water elevation by calculating the RMS error of water levels, the mean water level error (ME), and the peak water elevation error (PE). For a comparison the Skill is calculated, too. Among these metrics, the PE defined as the maximum modeled water elevation minus the maximum observed elevation, has the most important impact on coastal flooding caused by storm tides. The RMSE indicates the average deviation of the modeled water levels (η_{model}) from the observations (η_{obs}) and is computed as

$$RMSE = \left[\frac{1}{N}\sum_{i=1}^{N}(\eta_{model} - \eta_{obs})^2\right]^{1/2} \quad (3)$$

here, N is the number of data points. The mean error (ME) is defined as

$$ME = \frac{1}{N}\sum_{i=1}^{N}(\eta_{model} - \eta_{obs}) \quad (4)$$

The Skill evaluates the coherence between the model results and observations. Using a method presented by Wilmott (1981) we define

$$Skill = 1 - \frac{\sum_{i=1}^{N}(\eta_{model} - \eta_{obs})^2}{(|\eta_{model} - \bar{\eta}_{obs}| + |\eta_{obs} - \bar{\eta}_{obs}|)^2} \quad (5)$$

where $\bar{\eta}_{obs}$ is the time mean. Perfect agreement between model results and observations will yield a skill of one and complete disagreement yields a skill of zero.

Results of the local model runs are evaluated for control stations as shown in Fig. 9 and in Table 3. Except for few larger peak errors at stations MAC and QUB during Typhoon Dujuan, and at station QUB during Typhoon Hagupit (Table 3, without background wind), the PE at other stations during the nine typhoons is captured within 0.23 m. High RMSE (max. 0.85 m) and ME (min. -0.49 m) are found at station TBT in modeled negative surges in Shenzhen Bay due to overestimated winds during super Typhoons Mangkhut and Hato; the rest of RMSE in all runs is less than 0.28 m. Absolute values of ME estimated during typhoons that made landfall on the left bank of the PRE is generally larger than that during typhoons making landfall on the right bank. Overall, the model performance during Typhoon Dujuan is not as good as that during other typhoons due to the high PE.

A smaller PE does not ensure a smaller RMSE, and vice versa; such as that shown at station TBT during typhoons Mangkhut or Hato and that at station QUB during Dujuan or Hagupit. Even for the same RMSE the PE differs greatly. The smaller the RMSE, the larger the Skill. When the RMSE is less than

0.25 m, the Skill is greater than 0.95 (Table 3), the model results are more consistent with the observations.

Table 3. Statistical assessments of model performance

Station	Typhoon	Peak Error (m)	Mean Error (m)	RMS Error (m)	Skill	Typhoon	Peak Error (m)	Mean Error (m)	RMS Error (m)	Skill
MAC	Imbudo	0.13	0.06	0.24	0.968	Mangkhut	n/a	n/a	n/a	n/a
TBT		-0.11	-0.03	0.27	0.944		0.04	-0.49	0.85	0.797
QUB		-0.03	0.10	0.18	0.966		0.00	-0.23	0.29	0.954
MAC	Hagupit	0.04	-0.07	0.14	0.994	Utor	-0.02	-0.10	0.18	0.979
TBT		-0.04	-0.05	0.17	0.989		0.00	0.05	0.18	0.986
QUB		-0.32	-0.11	0.17	0.986		-0.06	-0.03	0.11	0.992
MAC	Hagupit	0.11	-0.01	0.12	0.995	Dujuan	0.50	0.06	0.26	0.941
TBT	with back-	0.03	-0.01	0.17	0.988		-0.01	-0.14	0.23	0.965
QUB	ground wind	-0.23	-0.06	0.13	0.991		0.31	0.03	0.26	0.924
MAC	Koppu	-0.04	0.03	0.15	0.991	Usagi	-0.01	-0.13	0.21	0.962
TBT		-0.14	-0.02	0.16	0.988		-0.15	-0.10	0.19	0.982
QUB		-0.05	0.01	0.12	0.989		0.04	-0.10	0.21	0.949
MAC	Hato	0.02	n/a	n/a	n/a	Nida	0.11	0.05	0.12	0.991
TBT		-0.09	-0.13	0.40	0.939		-0.17	0.09	0.15	0.991
QUB		0.18	0.03	0.13	0.991		0.23	0.12	0.15	0.985

We note that just before and after Typhoon Utor made landfall on the left bank, most of the waters in the PRE were within its center ($r_{min}/R_{mw} < 0.5$, Table 1); winds over there were not strong, and no minimum RMSE was found from Eq. (2). K_L is determined by referring to the wind reduction factor of other typhoons that made landfall on the left bank and to the difference in K_L between typhoons making landfall on the right and the left banks of the PRE. In this case, storm surges in the PRE were mainly generated by the central low pressures and well reproduced, see Fig. 9, with absolute PE less than 0.1 m, RMSE less than 0.2 m, and Skill greater than 0.98 at control stations. This verifies the effectiveness of modeling storm surges caused by atmospheric pressure gradients shown in Eq. (A1).

EFFECTS OF WAVES ON STORM TIDE LEVELS

Wave induced forces is taken into account by coupling the storm tide model to SWAN wave model with default settings to test effects of waves on storm tide levels; thus, the wave model runs without efforts to calibrate it in this study. Being different from the regional and local storm tide models that operate independently, the wave simulation adopts a local finer grid nested in a regional model to run. The local and regional grids of wave model have similar domains and grid sizes to that of local and regional storm tide models.

Wind conditions are different during typhoons that made landfall on the right and left banks of the PRE, and wind fields generated in the PRE change drastically in space and time during typhoons as well. Accordingly, both stationary and nonstationary wave modes are tested first in the wave simulation for Typhoons Hagupit and Usagi, which made landfall on the right and left banks of the PRE respectively. A good agreement is found between the modeled and observed maximum significant wave heights (H_s) by using the stationary mode (Fig. 10). This mode is then used to simulate waves generated by the selected nine typhoons.

Results of flow-wave coupling simulation show that, during typhoons that made landfall on the right bank of the PRE, noticeable wave setups are found on both sides of the lower reach of the PRE, but it increases more along the right side. Wave setups during typhoons that made landfall on the left bank are insignificant and can be ignored.

In the PRE, effects of waves on storm tide levels depend on the path, intensity, and size of a storm. For example, waves generated by super Typhoon Mangkhut increased maximum storm tide levels at station MAC on the right side of PRE and at station TBT on the left side by about 0.17 m and 0.15 m respectively. During Typhoon Hagupit wave setups were mainly found along the right side of the lower reach of the PRE, the increase in peak water levels due to wave actions at stations MAC and TBT was about 0.2 m and 0.07 m respectively. A maximum wave setup was found about 0.3 m in waters adjacent to the mouth of Xi river to the west of the PRE during Typhoons Hagupit, Hato, and Mangkhut (note that the river runoff was not incorporated into the modeling in this study). This is likely caused by sand bars

accumulated in waters close to the river mouth, which makes local seabed changed drastically. Studies have shown that wave contribution to storm surge highly depends on the slope and depth of the sea bottom (Resio and Westerink, 2008).

Due to wave setups, K_L estimated for typhoons making landfall on the right bank of the PRE may need to be adjusted slightly lower. Like the storm surge, the wave is also sensitive to the change of K_L; this adjustment should take account of the wave model calibration.

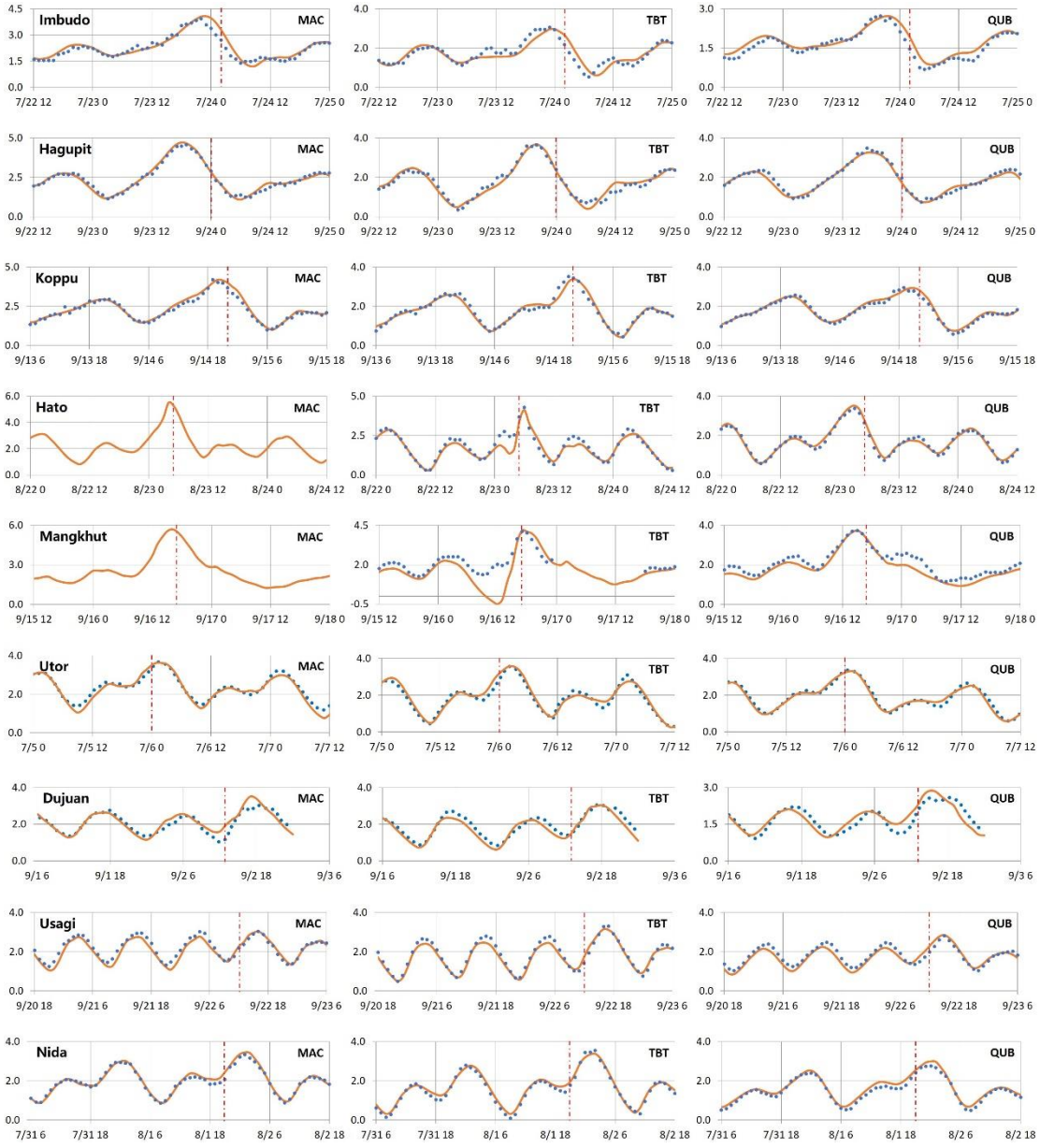

Legend: ..... observed —— modeled dashed vertical line – landfall time

Figure 9 - Model evaluation for storm tide elevation at control stations during selected nine typhoons

DISCUSSIONS AND CONCLUSIONS

By reviewing the three metrics for evaluating the model performance, one sees that the model underestimates the storm tide peak and mean water elevations at station QUB during Typhoon Hagupit. As a trial run, we increase the wind speed far away from the eyewall of the storm while keeping the modeled maximum wind unchanged by setting observed winds at station WAG as the model background wind (using the built-in wind module of WES, Deltares, 2016), see Fig. 12. As a result, the model performance improves markedly by reducing PE from -0.32 m to -0.23m, and ME from -0.11 m to -0.06

m (Table 3). Because the minimum relative distance (r_{min}/R_{mw}) to control stations was about 3 (Table 1), in most of time when the typhoon hit the PRE the distance was further. Therefore, the wind speed modeled in this distance is underestimated by the parametric model, resulting in large errors in modeled storm tide elevations.

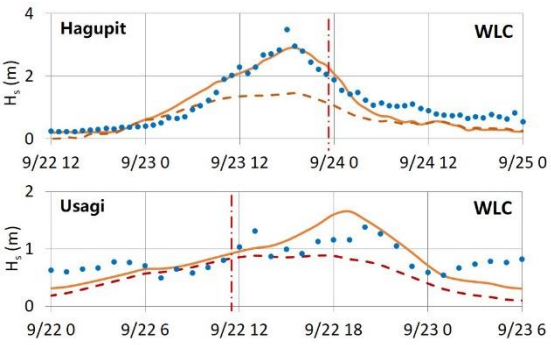

Legend: ..... observed ——— stationary mode
- - - - - non-stationary mode

Figure 10 - Evaluation of wave heights (H_s) with stationary and nonstationary wave modes

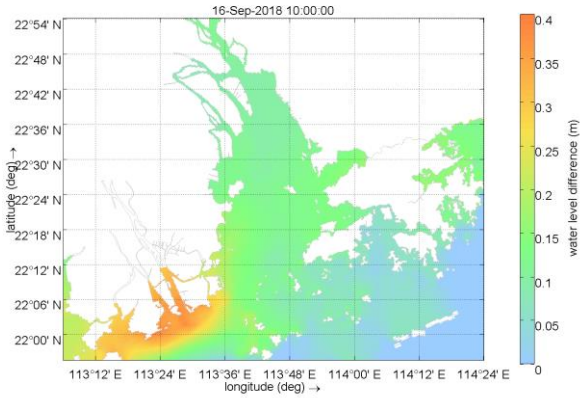

Figure 11 - Distribution of wave setups during Typhoon Mangkhut

Similarly, the r_{min}/R_{mw} during Typhoon Imbudo was greater than 3.8 (Table 1); this leads to a large K_L determined by finding the minimum RMSE of the highest storm tide levels in order to compensate for the modeled lower wind speed. But the reason for a larger K_L found for super Typhoons Hato and Mangkhut is likely that the wind drag coefficient is limited by the capped wind speed representation (Powell et al. 2003; Makin 2005).

When most of the PRE is within the R_{mw} ($r_{min}/R_{mw} < 1$) of a typhoon, wind speed and direction that change rapidly in space and time inside the typhoon eyewall may be modulated by mountains and skyscrapers around the PRE. The smaller the radius, the greater the impact on winds; then the winds are unlikely be simulated satisfactorily. Combined with the deficiency of Holland (1980) model in reproducing the core wind structure, these may account for the poor performance of storm tide simulation during typhoon Dujuan.

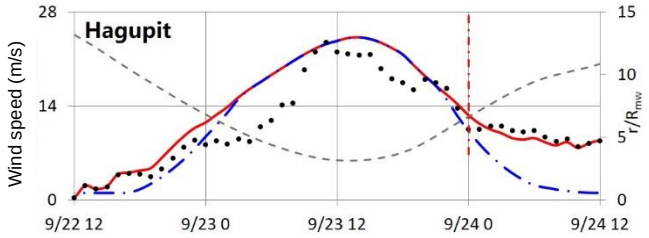

Legend: ..... observed ——— after adjustment – · – · before adjustment

Figure 12 - Adjustment of modeled winds by setting observed winds at station WAG as model background wind

In some cases, even if modeled winds are stronger than actual winds modulated by natural and built environment, the impact on storm tide levels is local. For instance, winds overestimated locally at station TBT during super Typhoons Hao and Mangkhut cause simulated storm tides with large RMSE at the station, but this does not greatly affect the model performance in prediction of the storm tide peak elevation.

In other cases, therefore, by referring to the approach discussed in this study to determine the three wind parameters, it is applicable and effective to use the Holland (1980) model for modeling storm tides, especially peak storm tide elevations in the PRE.

Depending on the track and maximum surface winds of a storm, the wind reduction factor considering the orographic effect is about 0.65 ~ 0.7 for typhoons that made landfall on the right bank of the PRE, and 0.5 ~ 0.55 for typhoons making landfall on the left bank. The K_L derived from a flow-wave

coupling simulation shall be closer to the true value, but the one estimated without taking account of wave effects can be used conveniently to approximate the storm tide simulation. The radius to maximum winds can be efficiently adjusted according to observed pressures through the exponential distribution of atmospheric pressure field; and the peakedness is verified on the basis of maximum wind speed versus pressure drop relations.

As a prerequisite for good model performance, the grid size somewhere in a storm tide model shall be smaller than the minimum spacing among soundings points at that location in order to effectively produce the bathymetry described by the soundings data. Both RMSE and PE shall be used for evaluating the performance of storm tide modeling, though the RMSE alone is conventionally used in the tidal simulation. Since the highest storm tide level has a greater impact on coastal floodings, the PE shall have a higher weight.

APPENDIX

Parametric Wind Model

The Holland (1980) model provides a wind field directly from input values of R_{mw} and storm central pressure p_c. It is based on the exponential distribution of the atmospheric pressure field proposed by Schloemer (1954) with the addition of a peakedness parameter B,

$$\frac{p - p_c}{p_n - p_c} = exp\left[-\left(\frac{R_{mw}}{r}\right)^B\right] \tag{A1}$$

where p is the pressure at radial distance r from the center, p_n is the ambient pressure. The wind speed distribution in the radial direction is determined from the equilibrium between the centrifugal force of a rotating air mass with the atmospheric pressure gradient and the Coriolis forces. The resulting wind speed is called the gradient wind speed and is given by

$$V_g = \sqrt{\frac{B(p_n - p_c)}{\rho}\left(\frac{R_{mw}}{r}\right)^B \exp\left[-\left(\frac{R_{mw}}{r}\right)^B\right] + \frac{r^2 f^2}{4}} - \frac{rf}{2} \tag{A2}$$

where f is the Coriolis parameter and ρ is air density. Eq. (A2) provides a radially symmetric profile of estimated gradient level winds which must be transferred to the +10 m reference surface by the surface wind reduction factor K_m.

$$V_s = K_m V_g \tag{A3}$$

Harper and Holland (1999) suggested that K_m can be considered as approximately 0.7 over the ocean, and V_s is to be considered as a 10-minute averaged wind sample. An empirical relation for B is also proposed as

$$B = 2 - \frac{p_c - 900}{160} \qquad 1.0 < B < 2.5 \tag{A4}$$

With B_s introduced for surface data, Eq. (A2) may be used to estimate the surface wind (Holland, Belanger, and Fritz 2010). At $r = R_{mw}$, neglecting Coriolis terms, as it is relatively small compared to the pressure gradient and centrifugal forces near R_{mw}, then

$$B_s = \frac{V_{ms}^2 \rho_{ms} e}{p_{ns} - p_{cs}} \tag{A5}$$

where the subscript s refers to surface values (at a nominal height of 10 m). If the maximum surface winds V_{ms} and central pressure p_{cs} have been directly or reliably independently observed, then Eq. (A5) can be used to estimate the parameter B_s.

Adjustment of Modeled Winds

The parametric wind model assumes a circular wind flow pattern and doesn't properly depict the actual surface wind directions due to the bottom friction resistance, which point toward the center of the storm at a deflected angle. For a stationary tropical cyclone, the inflow angle β at the surface is suggested by Bretschneider (1972) as a function of r as

$$\begin{aligned} \beta &= 10^o\left(1+\frac{r}{R_{mw}}\right)0 && r < R_{mw} \\ \beta &= 20^o + 25^o\left(\frac{r}{R_{mw}}-1\right) && R_{mw} \le r < 1.2R_{mw} \\ \beta &= 25^o && r \ge 1.2R_{mw} \end{aligned} \qquad \text{(A6)}$$

where β is measured inward from the isobars. Based on Eq. (A6), β varies linearly from 10^o at the center to 20^o at R_{mw}, then increases linearly to 25^o at $1.2R_{mw}$, and remains at 25^o beyond $1.2R_{mw}$.

In addition, the parametric wind field defined by Eq. (A2) is axisymmetric; it cannot represent the asymmetry of real wind fields, which are intrinsically related to the 3-dimensional structure of the storm, its forward motion speed, the underlying surface conditions, and the atmospheric environment within which the cyclone is embedded. This asymmetry is currently approximated by the resultant of forward and circular wind motion. In the Northern Hemisphere, tropical cyclone winds spin in the counter-clockwise direction. The forward motion of a tropical cyclone increases the wind speed in the right quadrants and decreases the wind speed on the left. This provides a left-right asymmetric wind field. It has no consensus on how to consider the influence of forward motion on winds of different positions. In this study we follow the Jelesnianski's (1966) approach, which suggests that the influence of forward motion on winds of different radii is taken account by a correction term

$$\boldsymbol{U}_f = \frac{R_{mw}\, r}{R_{mw}^2 + r^2}\boldsymbol{V}_f \qquad (A7)$$

where $\mathbf{V}_f$ is the forward motion velocity of a storm. The correction term $\mathbf{U}_f$ is then vectorially added to the axisymmetric wind velocity computed from the parametric wind model. The term is equal to zero at the center of the storm and increases to a maximum of $0.5V_f$ at R_{mw}, and then decreases radially outward. Recent research (Ling and Chavas 2012) shows that the correction term reaches the maximum value of $0.67V_f$ at $1.38R_{mw}$, and then taking the value 0.5~0.6 V_f. Although it is still inconclusive about the correction value, the effect due to its uncertainties on the wind field is insignificant. The adjusted winds show approximately the asymmetry of the real wind field (Fig. 5).

REFERENCES

Bomers, A., Schielen, R.M.J., and Hulscher, S.J.M.H. 2019. "The influence of grid shape and grid size on hydraulic river modeling performance." *Environmental Fluid Mechanics* 19 (449). https://doi.org/10.1007/s10652-019-09670-4.

Bretschneider, C.L. 1972. "A non-dimensional stationary hurricane wave model." *Proceedings of the Offshore Technology Conference* vol. I: 51–68.

Delft Hydraulics. 2008. Pearl River Delta Water Quality Model: Final Study Report. EPD, HKSAR.

Deltares. 2016. Wind Enhance Scheme for Cyclone Modelling-User Manual, Version: 3.01, Revision 47282. Delft, Netherlands.

Egbert, G. D., and Erofeeva, S.Y. 2002. "Efficient Inverse Modeling of Barotropic Ocean Tides." *Journal of Atmospheric and Oceanic Technology* Vol: 19, 183–204, DOI: https://doi.org/10.1175/1520-26(2002)019<0183:EIMOBO>2.0.CO;2

Holland, G.J. 1980. "Analytical Model of the Wind and Pressure Profiles in Hurricanes." *Monthly Weather Review* Vol. 108: 1212-1218.

Holland, G.J. 2008. "A Revised Hurricane Pressure–Wind Model." *Monthly Weather Review* 136: 3432–3445.

Holland, G. J., Belanger, J. I., and Fritz, A. 2010. "A revised model for radial profiles of hurricane winds." *Monthly Weather Review* 138: 4393–4401. doi:10.1175/2010MWR3317.1.

Jarosz, E., Mitchell, D. A., Wang, D.W., and Teague,W. J. 2007. "Bottom-Up Determination of air-sea Momentum Exchange Under a Major Tropical Cyclone." *Science* 315: 1707–1709.

Jelesnianski, C.P. 1966. "Numerical computations of storm surges without bottom stress." *Monthly Weather Review* 94 (6): 379–394.

Hong Kong Observatory. 2001. "Tropical Cyclones affecting Hong Kong in 2001." Section 3 in *Tropical Cyclones* in 2001.

Hong Kong Observatory. 2017. "Tropical Cyclones affecting Hong Kong in 2017." Section 3 in *Tropical Cyclones* in 2017.

Hong Kong Observatory. 2018. “Tropical Cyclones affecting Hong Kong in 2001.” Section 3 in *Tropical Cyclones* in 2018.

Knaff, J.A., Harper, B.A. 2012. Tropical Cyclone Surface Wind Structure and Wind-Pressure Relationships. *Seventh International Workshop on Tropical Cyclones*, WMO.

Harper, B.A., and Holland, G.J. 1999. “An updated parametric model of the tropical cyclone.” *Proceedings of the 23rd Conference of Hurricane and Tropical Meteorology*: 893–896. Dallas, Texas.

Kohno, N., Dube, S., Entel, M., Fakhruddin, S., Greenslade, D., Leroux, M.D., Rhome, J., and Nguyen, T. 2018. “Recent progress in storm surge forecasting.” *Tropical Cyclone Research and Review* 7 (2): 128-139. doi:10.6057/2018TCRR02.04.

Lau, D.S., and Chan, S.T. 2017. Storm Surge in Hong Kong associated with Super Typhoon Hato (1713). 4th International Workshop on Tropical Cyclone Landfall Processes (IWTCLP-4), Macau, China.

Ling, N., and Chavas, D. R. 2012. “On hurricane parametric wind and applications in storm surge modeling.” Journal of Geophysical Research.” 117, D09120. doi:10.1029/2011JD017126.

Makin, V. K. 2005. “A note on the drag of the sea surface at hurricane winds.” *Boundary-Layer Meteorology* 115 (1):169–176.

Li, L., Yang, J., Lin, C.Y., Chua, C.T., Wang, Y., Zhao, K., and Wu, Y.T. et al. 2018. “Field survey of Typhoon Hato (2017) and a comparison with storm surge modeling in Macau.” *Nat. Hazards Earth Syst. Sci*. 18:3167–3178. https://doi.org/10.5194/nhess-18-3167-2018.

Powell, M. D., Vickery, P. J., and Reinhold, T. A. 2003. “Reduced drag coefficient for high wind speeds in tropical cyclones.” *Nature* 422, 279-283.

Powell, M.D., Soukup, G., Cocke, S., Gulati, S., Morisseau-Leroy, N., Hamid, S., Dorst, N., Axe, L. 2005. “State of Florida hurricane loss projection model: atmospheric science component.” *Journal of Wind Engineering and Industrial Aerodynamics* 93: 651–674

Resio, D.T. and Westerink, J.J. 2008. “Modeling the Physics of Storm Surge.” *Physics Today* September, 33–38.

Schloemer, R.W. 1954. Analysis and synthesis of hurricane wind patterns over Lake Okechobee, FL. Hydromet Report No. 31, Government Printing Office, Washington, D.C.

Shen, Q. 2022. “Location of open boundary and its Effects on Model Performance.” *Proceedings of the 39th IAHR World Congress* pp.5456-5465, Granada, Spain. doi://10.3850/IAHR-39WC2521716X202257.

Vickery, P. J., Masters, F.J., Powell, M.D., and Wadhera, D. 2009. “Hurricane hazard modeling - The past, present, and future.” *Journal of Wind Engineering and Industrial Aerodynamics* 97:392–405.

Vickery, P.J., Wadhera, D. 2008. “Statistical models of Holland pressure profile parameter and radius to maximum winds of hurricanes from flight level pressure and H *Wind data.” *Journal of Wind Engineering and Industrial Aerodynamics* 47:2417–2497.

Willmott, C. J. 1981. “On the validation of models.” *Physical Geography* 2(2): 184-194. https://doi.org/10.1080/02723646.1981.10642213.

Willoughby, H.E., and Rahn, M.E. 2004. “Parametric representation of the primary hurricane vortex. Part I: Observations and evaluation of the Holland (1980) model.” *Monthly Weather Review* 132:3033–3048.

Zheng, P., Li, M., Wang, C.X., Wolf, J., Chen, X., Dominicis, M.D., Yao, P., and Hu, Z. 2020. “Tide-Surge Interaction in the Pearl River Estuary: A Case Study of Typhoon Hato.” *Frontiers in Marine Science* 7:236. doi: 10.3389/fmars.2020.00236.